August 27-31, 2023
FLORENCE - ITALY
ICWE 16
16th International Conference on Wind Engineering

The linear-time-invariance notion to the Koopman analysis: decouple and quantify the cause-effect relationships of fluid-structure interactions

Cruz Y. Li [1,2], Zengshun Chen [1], Tim K.T. Tse [2], Xuelin Zhang[3], Yunfei Fu[2], Xisheng Lin[2], Yixiang Wang[2], Ziyue Peng[2]

[1]Chongqing University, Chongqing, China, yliht@connect.ust.hk; zchenba@connect.ust.hk
*[1]The Hong Kong University of Science and Technology, Hong Kong, China, timkttse@ust.hk; yfuar@connect.ust.hk; xlinbl@connect.ust.hk; ywanghr@connect.ust.hk; ziyue.peng.daniel@gmail.*com; School *of Atmospheric Sciences, Sun Yat-sen University, Zhuhai, China, zhangxlin25@mail.sysu.edu.cn*

SUMMARY:
Based on our serial research on the linear-time-invariance (LTI) notion of the Koopman analysis (Koopman-LTI) (Li et al., 2022 *Physics of Fluids*, 34(12) 125136; Li et al., 2023 *Journal of Fluid Mechanics*, Accepted in Press), this paper presents a computer-aided Koopmanistic approach to statistically decouple, quantify, and elucidate the cause-and-effect relationships of fluid-structure interactions (FSI). Applied Koopmanism is the derivation of a finite approximation of a Hamiltonian (i.e., the Koopman operator) that globally and optimally linearizes a finite nonlinear system at the cost of raising its dimensionality to infinity. The operator could then be tangibly attained and accurately approximated by data-driven Koopman models on finite manifolds. Demonstrated via a pedagogical prism wake, the new approach involves four steps: isolation, matching, visualization, and quantification. Results disclosed the subcritical wake's six predominant, low-order excitation-response mechanisms of two classes. Class 1 contains two mechanisms that describe 1) the forced-separation-induced asymmetric wall jet, shear-layer formation and development, and subsequent Bérnard-von Kármán vortex shedding, and 2) the turbulence production, negative-production cavity, and fluid entrainment. Class 2 contains 4 mechanisms that all trace back to the harmonic waves of turbulence initialization and cascade, namely the second-harmonic, sub-harmonic, and two ultra-harmonics. The underlying physics of the two classes was identified, and their contribution to the overall FSI system was quantified. Furthermore, the defining difference between the classes was unveiled through an analysis of the response-to-excitation ratio. Of its data-driven nature, the Koopman-LTI applies to many FSI and bluff-body problems in wind engineering, if not many other nonlinear and stochastic physical systems in general.

Keywords: Fluid-structure interaction, Data-driven analysis, Applied Koopmanism, Koopman-LTI

1. INTRODUCTION

Studying fluid-structure interaction (FSI) is extremely difficult due to fluid's nonlinearity, scale & dimensionality, and stochasticity; it involves linearization, order reduction, spectral isolation, statistical quantification, and phenomenological visualization. To this end, one of the latest cutting-edge developments in fluid mechanics and data science, applied Koopmanism (Budišić et al., 2012), bears vast promise. Li et al. (2023b) offered a comprehensive review of the Koopman analysis and its subordinate algorithm, the Dynamic Mode Decomposition (DMD), for wind engineering applications. This article outlines a novel conception and methodology that can

decouple FSI systems and statistically quantify each fluid-structure pair's (i.e., excitation-response mechanism) contribution, and demonstrates this framework via a pedagogical prism wake. The approach is named the linear-time-invariance notion of the Koopman analysis (Koopman-LTI) (Li et al., 2022; 2023a). Of its data-driven nature, the Koopman-LTI applies to many FSI and bluff-body problems in wind engineering.

2. METHODOLOGY

2.1. Test Subject

The prism wake, a classical free-shear flow at Re=2.2×10^4 with inhomogeneous, anisotropic wake turbulence and no initial perturbation, was selected as the test subject. The case was numerically simulated by large-eddies simulations (LES) with near-wall resolution. The case has also been validated by stringent CFD standards, rendering its accuracy comparable to several direct numerical simulations (DNS). Details can be found in Li et al. (2022b).

2.2. Decoupling FSI

Fig. 1 (left) presents the conceptual rundown of the Koopman-LTI, involving four steps: 1) isolating temporally orthogonal modes by a globally optimal linear model; 2) matching flow field and wall pressure modes—those embodying excitation and response mechanisms—into frequency-matching fluid-structure pairs; 3) visualizing the pairs' instantaneous phenomenology to underpin the associated phenomena and cause-and-effect relationships; 4) quantifying each pair's statistical contribution to the overall spatiotemporal content. The modular Koopman-LTI architecture is presented in Fig. 1 (right); the DMD is only one of many substitutable data-driven algorithms to approximate the Koopman operator and its eigen tuples on a finite manifold.

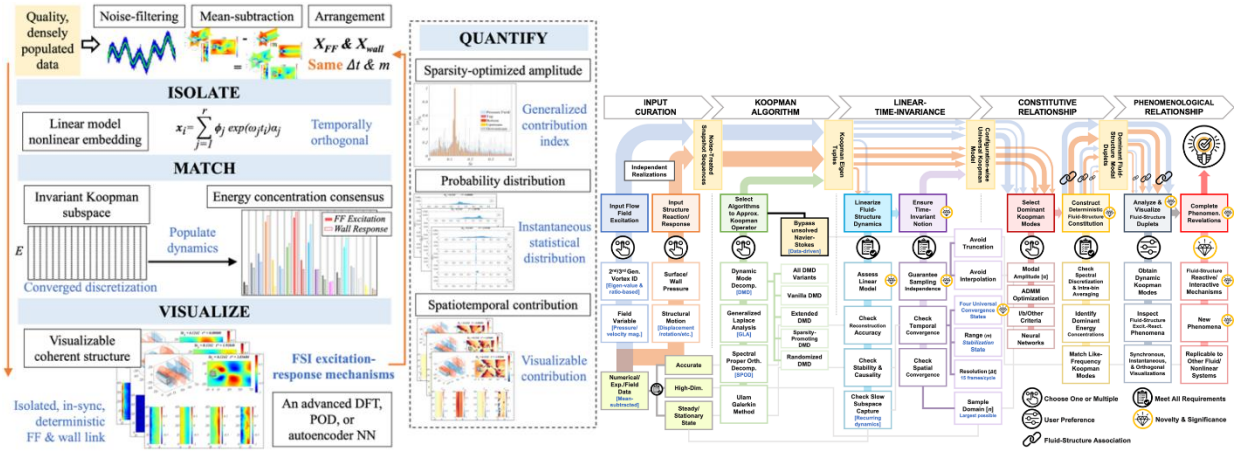

Figure 1. The conceptual rundown (left) and modular architecture (right) of the Koopman-LTI.

3. RESULTS AND DISCUSSION

3.1. Matching Fluid-Structure Pairs

The matching step involves the manual or computer-aided identification of dominant, like-frequency Koopman eigen tuples on a uniform Fourier spectrum that spans the observable

dictionary (see Fig. 2). Six low-order fluid-structure pairs were identified for the subcritical prism wake, representing the six predominant FSI excitation-response mechanisms. The six pairs could also be categorized into two classes: 1) Class 1 – mostly affecting the on-wind (i.e., upstream and crosswind) walls at *St*=0.0497 and 0.1242 (sky blue); 2) Class 2 – mostly affecting the downstream wall at *St*=0.0683, 0.1739, 0.1925, and 0.2422 (beige).

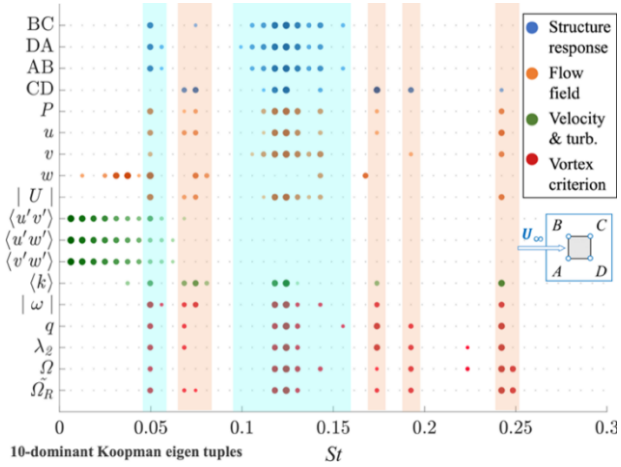

Figure 2. Koopman modes with the highest normalized amplitude on a uniform Fourier spectrum.

3.2. Phenomenological Analysis for Physics Implications

The visualization step studies the six low-order fluid-structure pairs to pinpoint exactly which phenomena they each characterize. Fig. 3 presents an example analysis for the fluid-structure pair at *St*=0.1242. The structures stem from the two shear layers that separate the fast external streams and the slow separation bubbles due to asymmetric wall jets forming at the leading edges. The phenomenological analysis suggests that the fluid-structure pair at *St*=0.1242 describes shear layer and wake behaviors throughout a Bérnard-von Kármán vortex shedding cycle, from the initial forced separation to the subsequent shear layer development, then to the reattachment-induced shedding, and ultimately to the culmination into Kármán vortices.

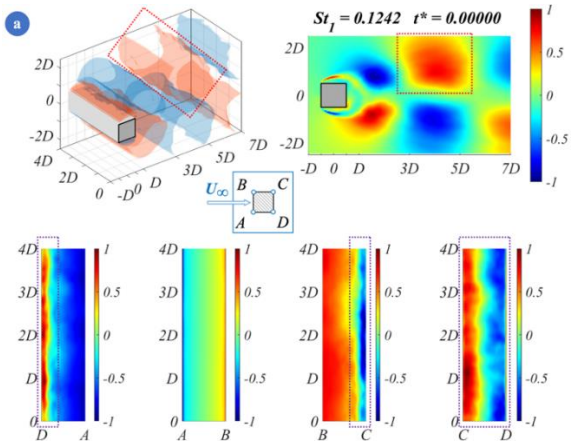

Figure 3. Fluid-structure paired Koopman mode of |*U*| with *St*=0.1242 at *t**=*tD*/*U*∞=0.0000.

3.3. Quantifying Koopman pair's contribution to overall FSI

The quantification can be conducted through evaluating a Koopman mode's coefficient of weight with respect to the overall spatiotemporal sum (Eq. (1)), or through contribution at every time instant for every node (Eq. (2)):

$$A_j = \alpha_j \Big/ \sum_{k}^{r} \alpha_k \,. \tag{1}$$

$$C_{i,j} = \phi_j \, exp(\omega_j t_i)\alpha_j \Big/ \sum_{k=1}^{r} \phi_k \, exp(\omega_k t_i)\alpha_k. \tag{2}$$

where r is the truncation order, ϕ_j is the Koopman eigen function, ω_j is the eigen frequency, t_j is a time instance within the sampled span, and α_j is the coefficient of weight.

Table 1 summarizes Class 1's contribution by the sparsity-promoting Dynamic Mode Decomposition (SPDMD) from the perspective of Koopman mode's coefficient of weight. The *St*=0.1242 mode cluster contributes 15.7% to the flow field, but its contribution is 45.4% to the upstream wall (i.e., AB), 31.7% to the crosswind walls (i.e., DA and BC), and 14.7% to the downstream wall (i.e., CD). The trend is consistent with the mode cluster at *St*=0.0497. Generally, Class 1 mechanisms may amplify excitation on the on-wind walls and downplay it on the downstream wall.

Table 1. Fluid-structure pairs' contribution to the overall FSI system by Koopman analysis via SPDMD (Class 1).

Fluid-Struct. Pair (*St*)	**Broad-band Modes**	***A* (%)**				
		DA	**AB**	**BC**	**CD**	**|*U*|**
0.0497	2	3.60	5.28	3.60	2.30	2.47
0.1242	10	31.7	45.4	31.7	14.7	15.7
Class 1 Sum	12	**35.3**	**50.7**	**35.3**	**17.0**	**18.1**

4. CONCLUSIONS

A computer-aided Koopmanistic approach is proposed, known as the Koopman-LTI, to statistically decouple, quantify, and elucidate the cause-and-effect relationships of FSI. Demonstrated via a pedagogical prism wake, results proved the effectiveness and insightfulness of the newly developed technique. Of its data-driven nature, the Koopman-LTI applies to the vast array of FSI and bluff-body problems in wind engineering, if not many other fluid domains.

REFERENCES

Budišić, M., Mohr, R., & Mezić, I., 2012. Applied Koopmanism. Chaos, 22(4), 047510.

Li, C. Y., Chen, Z., Lin, X., Weerasuriya, A. U., Zhang, X., Fu, Y., & Tse, T. K. T. (2022). The linear-time-invariance notion to the Koopman analysis: The architecture, pedagogical rendering, and fluid–structure association. Physics of Fluids, 34(12), 125136. https://doi.org/10.1063/5.0124914

Li, C. Y., Chen, Z., Tse, T. K. T., Weerasuriya, A. U., Zhang, X., Fu, Y., & Lin, X. (2022b). A parametric and feasibility study for data sampling of the dynamic mode decomposition: range, resolution, and universal convergence states. Nonlinear Dynamics, 107(4), 3683–3707. https://doi.org/10.1007/s11071-021-07167-8

Li, C. Y., Chen, Z., Tse, T. K. T., Weerasuriya, A. U., Zhang, X., Fu, Y., & Lin, X. (2023a). The Linear-Time-Invariance Notion of the Koopman Analysis-Part 2: Physical Interpretations of Invariant Koopman Modes and Phenomenological Revelations. Journal of Fluid Mechanics. Accepted in Press. https://arxiv.org/abs/2112.03029v1

Li, C. Y., Chen, Z., Zhang, X., Tse, T. K. T., & Lin, C. (2023b). Koopman analysis by the dynamic mode decomposition in wind engineering. Journal of Wind Engineering and Industrial Aerodynamics, 232, 105295. https://doi.org/10.1016/J.JWEIA.2022.105295